A parametric study of the head-on collision of normal shock waves in dusty gases

1988 Fluid Dyn. Res. 4 239

(http://iopscience.iop.org/1873-7005/4/4/A02)

Fluid Dynamics Research 4 (1988) 239–253
North-Holland

A parametric study of the head-on collision of normal shock waves in dusty gases

T. ELPERIN, G. BEN-DOR and O. IGRA

Pearlstone Center for Aeronautical Engineering Studies, Department of Mechanical Engineering, Ben-Gurion University of the Negev, Beer Sheva, Israel

Received 24 February 1988

Abstract. The effect of the various flow parameters, namely: the diameter of the solid particles, the material density of the solid particles, and the loading ratio of the solid particles on the flow field which is obtained when two normal shock waves collide head-on in a two phase dust–gas suspension has been investigated numerically, using the modified random choice method (RCM). The results were compared with those appropriate to the dust physical parameters used recently by Elperin, Ben-Dor and Igra in their study of the head-on collision of normal shock waves in dusty gases.

1. Introduction

The head-on collision of normal shock waves is a classical gas dynamics problem which was first studied in detail by Glass (1987), Gould (1952) and Nicholl (1951) more than three decades ago. Schematical illustrations of the waves in the (x, t)-plane and their location at a time before, t_1, and after, $t_2 > t_c$, the head-on collision time, t_c, are shown in figs. 1(a), (b) and (c), respectively.

Prior to the head-on collision, two shock waves, S_1 and S_2, propagate, one from left to right and the other from right to left into a quiescent gas, state (0). Two new thermodynamic states (1) and (2) are obtained behind S_1 and S_2, respectively. After the head-on collision the incident shock waves reflect back as new shock waves, S_3 and S_4, which now move apart, S_3 propagates towards the oncoming flow of state (1) and changes its properties to a new state, state (3), while S_4 propagates towards the oncoming flow of state (2) and changes its properties to a new state (4). States (3) and (4) are separated by a contact surface across which the pressure and the flow velocity are constant, but all the other flow properties, e.g., density, temperature, entropy, etc., are different. The contact surface can move either to the left or to the right depending on the strengths of the incident shock waves, S_1 and S_2. When the gas is pure, i.e., dust-free, the discontinuities (shock waves and contact surface) propagate with constant velocities, the flow states are uniform and the contact surface is infinitely thin. However, as shown by Elperin et al. (1987), when the gas is laden with dust particles, the velocities of the shock waves are not constant, the contact surface changes into a contact region and the flow states are not uniform anymore. In addition two solid particle trajectories are shown in fig. 1(a). The intersection of these two trajectories after the head-on collision of the two incident shock waves, which results in a multivalued solution, is discussed subsequently.

As mentioned earlier, the head-on collision of normal shock waves was first solved analytically by Glass (1987), Gould (1952) and Nicholl (1951). The solution is based on

0169-5983/88/$4.75

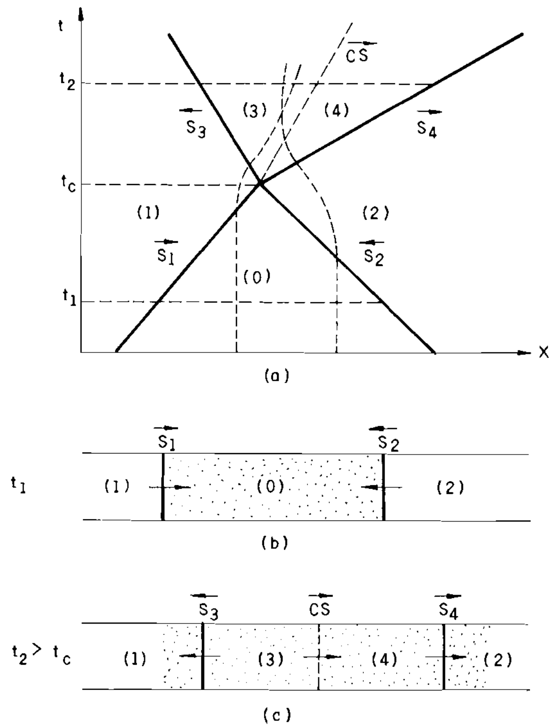

Fig. 1. Schematic illustration of the shock waves in the (x, t)-plane.

applying the well-known conservation equations for a normal shock wave Anderson (1982) separately across each of the incident and reflected shock waves and imposing the boundary condition of equal pressure and flow velocities on both sides of the contact surface.

In a recent study Elperin et al. (1987) have extended the solution of Glass (1987), Gould (1952) and Nicholl (1951), which is limited to the case of pure gases, to cover the more realistic case of gas-solid suspensions. This extension was motivated by the fact that wave interactions in two-phase flows are frequently encountered in nature and various technological applications. The presence of the solid particles results in considerable complications of the physical picture of the dusty gas flow compared to a pure gas flow, and, therefore, the mathematical description of the flow and the methods of solution are more complicated.

Unlike the solution of Glass (1987), Gould (1952) and Nicholl (1951) which was analytical, the solution of Elperin et al. (1987) was numerical. In their solution they applied the modified random choice method to obtain profiles of the various suspension properties at different times before and after the head-on collision. In their study they used only one set of dust parameters and hence only the effect of the dust presence on the obtained flow field was investigated. Their results clearly showed that the presence of the dust significantly affects the suspension flow field. Both the incident and reflected shock waves were found to move more slowly in dusty gases than in pure gases, the maximum pressures and temperatures were found to be higher in dusty gases, and the gas velocities were found to be lower. The aim of the present study is to investigate numerically the effect of the dust physical parameters on the obtained flow field in the suspension. The dust physical parameters as employed by Elperin et al. (1987) are used as a reference to which the results obtained in the present study, with different dust parameters, are compared.

General descriptions of gas-particle suspension models can be found in several review papers and books Soo (1967), Marble (1970) and Rudinger (1973). In a stationary flow the major difference between the case of a pure gas and that of a dusty gas is the existence of a relaxation zone behind the shock wave in the latter. The pioneering works of Carrier (1958), Kriebel (1964), Rudinger (1964), Schmitt-von Schubert (1969) as well as the work of Igra and Ben-Dor (1980) have all verified the existence of this relaxation zone and identified the parameters affecting it.

2. Present study

2.1. Assumptions

The subsequent analysis is based on the following assumptions which are usually used [Soo (1967), Marble (1970), Rudinger (1973), Carrier (1958), Kriebel (1964), Rudinger (1964), Schmitt-von Schubert (1969) and Igra et al. (1980)] when shock waves propagating into dust-gas suspensions are investigated.

The suspension is assumed to be composed of thermally and calorically perfect gas of constant viscosity and thermal conductivity and solid particles of spherical shape and equal diameter. The volume occupied by the particles is assumed to be negligibly small since their density is greater by orders of magnitude than that of the gas and the dust loading ratio is low. The gas and the particles interact with each other through the drag force, D, and the heat transfer rate, Q. The expressions for D and Q were adopted from Miura and Glass (1983), i.e.,

$$D = \tfrac{1}{8}\pi d^2 \rho (u - v) \, |u - v| \, C_D, \tag{1a}$$

$$Q = \pi d \mu \frac{C_\mathrm{p}}{\mathrm{Pr}} (T - \theta) \mathrm{Nu}, \tag{1b}$$

where

$$C_D = 0.48 + 28 \ \mathrm{Re}^{-0.58}, \qquad \mathrm{Nu} = 2.0 + 0.6 \ \mathrm{Pr}^{1/3} \ \mathrm{Re}^{1/2},$$

$$\mathrm{Re} = \rho \, |u - v| \, d/\mu, \qquad \mathrm{Pr} = \mu C_p/k.$$

In the above expression u and v are the velocities of the gas and the solid particles, T and θ are the temperatures of the gas and the solid particles, ρ is the density of the gaseous phase, d is the diameter of the dust particles, μ, k and C_p are the gas dynamic viscosity, thermal conductivity and specific heat capacity at constant pressure, respectively, C_D is the drag coefficient, Nu, Re and Pr are the Nusselt, the Reynolds and the Prandtl numbers, respectively.

Although the validity of the above phenomenological expressions describing the momentum and energy exchange between the gas and the solid particles can be questioned in some cases, the predictions of the suspension properties made on the basis of these expressions were found to be in reasonably good agreement with dusty shock tube experimental results Miura et al. (1983) and Sommerfeld (1985).

As can be seen from the expression for the drag force, D, the gravity effects, the Basset force and the force acting on the solid particles due to pressure gradients are assumed to be negligibly small. The latter assumptions are quite accurate when the solid–gas density ratio is large and pressure gradients are not high. Note that the assumption of small pressure gradients is valid behind the shock fronts. Across the shock fronts, however, $|\mathrm{d}p/\mathrm{d}x| \to \infty$, but since the size of the smallest solid particles used in the present study $d = 10$ μm is two orders of magnitude larger than the shock wave thickness which is of the order of 0.066 μm it can be assumed that the solid particles are unaffected when they pass through the shock fronts. Morgenthaler (1962) indicated that this is true even if the diameter of the solid particles is as small as 0.1 μm.

In addition to the above assumptions, the gas is assumed to be a continuous medium with a molecular mean free path much smaller than the diameter of the solid particles. As mentioned earlier, this assumption is valid for the particle diameters used in the present study. The effect of compressibility, i.e., the dependence of the drag coefficient and the Nu number on the Mach number can be also neglected for the considered range of flow Mach numbers (see Igra and Ben-Dor (1980)).

The expression for the heat transfer rate, Q, implies that only convective heat transfer is taken into account. Certainly, when the temperature of the particles becomes high enough, the radiative heat transfer becomes important Igra et al. (1980). Further to the above assumptions, it was also assumed that the temperature within the solid dust particles is uniform. This assumption is justified for the Biot number appropriate to the solid particles used in the present study is smaller than 0.1. Finally, it was assumed that the concentration of the solid phase is sufficiently low so that thermal (radiation) and momentum (collisions) exchange between the solid particles can be neglected.

It should be noted that while collisions between the solid particles are theoretically possible, the probability of such events is practically zero. This is verified by the fact that the mean free path of the solid particles, as calculated using elementary kinetic theory and the following typical dust parameters; $\beta = 1$, $\rho = 1.225$ kg/m^3, $d = 10^{-5}$ m and $\rho_s = 2.5 \times 10^3$ kg/m^3, is about 0.0034 m. This value is very large in comparison with the length scale of the interaction of the two shock waves. It should be further noted that the interaction between the solid particles becomes essential when the diameter of the solid particles is greater than 10^{-3} m. However, this critical diameter is greater by two orders of magnitude from the diameters used in the present numerical study. The fact that collisions between the solid particles can be neglected is used implicitly in the numerical solution. A gaseous suspension is modeled as a mixture of two interacting and mutually penetrating continua where particles do not interact with each other and do not contribute to the pressure. A discontinuous initial condition for the flow variables of the solid phase would result in a multivalued solution for the velocity of the solid phase. Since the flow variables of the solid phase are continuous, in the numerical solution we assumed a linear distribution of the flow variables of the solid phase between adjacent mesh points. This allows to preserve the first order accuracy of the random choice method and to avoid the difficulties associated with the multivalued solutions of the conservation equations for the solid phase.

The physical meaning of these multivalued solutions which are manifested by the intersection of the particles trajectories in the (x, t) plane is discussed below *. As the shock wave S_1 penetrates into the particle cloud, the particles are accelerated from left to right. In addition, the shock strength changes as it propagates because of the interaction with the particles and a reflected wave is created which modifies the particle's trajectories and finally returns into the pure gas, as indicated by the pressure variations in fig. 5a. If there were no reflected waves, all particle trajectories would be identical but shifted parallel to themselves because different particles are overtaken by the shock at different times. When the reflected waves are present there are slight differences between neighboring trajectories and intersections, leading to multivalued solutions, can occur. A similar situation takes place for the second shock wave S_2 which accelerates particles from right to left. After the interaction of the two shock waves, there are two interpenetrating particle clouds in regions (3) and (4), particularly near the point where the contact surface would be located in the case of a pure gas.

In this region particle trajectories intersect, and a multivalued solution occurs. Similar to the pure gas flow the latter creates the discontinuity in the flow of solid particles as was first pointed out by Kraiko (1979). However, since the number density of the solid particles is small,

* We are indebted to the unknown referee for his stimulating discussion of this subject.

the collisions between the particles in the thin transmission layer in the vicinity of the discontinuity are quite rare as was noted above. Therefore the flow pattern inside this transition layer will retain essentially its two-velocity character, i.e., two clouds of particles will penetrate through each other almost without collisions. This enables one to find the first order accurate solution of the Riemann problem for the solid particles flow by assuming linear distribution of the flow variables between adjacent nodes of the numerical mesh. Certainly when the mean free path of the solid particles becomes of the same order of magnitude as the characteristic length scale of the shocks interaction such an approach becomes rather inaccurate. Then the interaction between the particles at the discontinuities of the film or the cluster type [Kraiko (1982)] must be taken into account. The latter requires introducing additional assumptions into a two-fluid model of a suspension flow for closing the system of jump conditions on such discontinuities [Kraiko (1982)].

It should be noted that the solution of the conservation equations for the solid phase is of first order accuracy in time and spatial increments. Therefore, it is characterized by a relatively large numerical diffusion which is inherent in the adopted numerical scheme.

2.2. Conservation equations

Under the assumptions presented in the previous section, the one-dimensional non-stationary compressible flow of the gas–dust suspension is governed by the following system of partial (differential equations governed by the following system of partial differential equations expressing the conservation of mass, momentum and energy of the gaseous and the solid phases:

$$\frac{\partial \rho}{\partial t} + \frac{\partial}{\partial x}(\rho u) = 0, \tag{2}$$

$$\frac{\partial}{\partial t}(\rho u) + \frac{\partial}{\partial x}\left[\rho u^2 + P\right] = -\frac{\sigma}{m}D, \tag{3}$$

$$\frac{\partial}{\partial t}\left[\rho\left(C_v T + \tfrac{1}{2}u^2\right)\right] + \frac{\partial}{\partial x}\left[\rho u\left(C_p T + \tfrac{1}{2}u^2\right)\right] = -\frac{\sigma}{m}(vD + Q), \tag{4}$$

$$\frac{\partial \sigma}{\partial t} + \frac{\partial}{\partial x}(\sigma v) = 0, \tag{5}$$

$$\frac{\partial}{\partial t}(\sigma v) + \frac{\partial}{\partial x}(\sigma v^2) = \frac{\sigma}{m}D, \tag{6}$$

$$\frac{\partial}{\partial t}\left[\sigma\left(C_m\theta + \tfrac{1}{2}v^2\right)\right] + \frac{\partial}{\partial x}\left[\sigma v\left(C_m\theta + \tfrac{1}{2}v^2\right)\right] = \frac{\sigma}{m}(vD + Q), \tag{7}$$

where m is the mass of a solid dust particle ($m = \rho_s \pi d^3/6$ where ρ_s is the material density of the dust particles), C_v is the specific heat capacity of the gas at constant volume, C_m is the heat capacity of the solid particles, P is the suspension pressure, and σ is the spatial density of the solid phase. Note that the material and spatial densities of the solid phase are related through

$$\sigma = \frac{\pi d^3}{6} n_s \rho_s$$

where n_s is the number density of the solid particles.

2.3. Numerical technique

The above system of partial differential equations was solved numerically by the modified random choice method (RCM) with operator splitting technique.

The random choice method represents the combination of the explicit first order finite difference scheme [Godunov (1959)] and the Monte Carlo method. The random choice method has been used extensively in gasdynamics [Miura et al. (1983); Saito et al. (1984) and Miura et al. (1986)]. However, the random choice scheme employed in this research comprises some modifications which considerably improve the quality of the results. The main advantage of the random choice method over other numerical schemes is that it allows high resolution of shock waves and contact surfaces, while in other finite difference methods they are usually smeared over many grid points as a consequence of artificial viscosity and truncation error of the scheme. The random choice method utilizes the exact solution of the Riemann problem, i.e., initial value-problem for the hyperbolic system of partial differential equations (2)–(7) with piecewise constant initial data for a finite difference solution of the hyperbolic equations of gasdynamics. The Riemann problem is solved repeatedly between each pair of neighboring spatial grid points. The successive positions of the discontinuities (shock waves, etc.) between these mesh points are sampled with the help of the uniformly distributed sequences of Van der Corput [Elperin and Igra (1986)]. This implementation of uniformly distributed sequences considerably reduces the numerical noise and thus improves the quality of the results (for more details see, Elperin et al. (1986)).

Some other important details of the random choice scheme applied in the calculations are elaborated in the following. The solution of the Riemann problem with piecewise constant initial data was performed by the iterative method suggested first by Godunov (1959). The homogeneous part of eqs. (2)–(7) was solved by the random choice method. The general solution is obtained with the aid of operator-splitting technique, i.e., by solving alternately in each time step the two systems of differential equations. The first system of partial differential equations is derived from (2)–(7) with the right hand side omitted and is solved via the random choice method. The second system of equations is derived from eqs. (2)–(7) by omitting the spatial derivatives. The resulting system of ordinary differential equations is then solved with the initial data obtained from the random choice solution by Euler method. In the calculations the transmissive boundary conditions were assumed for the gaseous and the solid phases in order to avoid effects of waves reflected from the ends of the duct. The transmissive boundary conditions imply that $u_1 = u_2$ and $u_N = U_{N-1}$ where "1" and "N" are the two extreme mesh points. Physically this boundary condition simply states that we cut off a finite region from an infinite flow field and seek for the solution inside this region only. The absence of wave reflections from the end of the region covered by the calculations implies a duct of sufficient length beyond the numerical boundary that such reflected waves would arrive much to late to be of concern here.

The initial value problem with piecewise constant initial data for eqs. (5)–(7), describing the flow of the solid particles, was treated analytically Miura et al. (1983), assuming the linear distribution of flow variables between adjacent grid points. This approach enables one to preserve the first order accuracy of the method and avoids the difficulties arising as a result of the multivalued solution of eqs. (5)–(7).

All the thermodynamic and dynamic variables in eqs. (1)–(7) were presented in a nondimensional form as follows:

$$\begin{aligned}
&\bar{P} = P/P_0; \qquad \bar{\rho} = \rho/\rho_0; \quad \bar{\sigma} = \sigma/\rho_0;\\
&\bar{u} = \sqrt{\gamma}\,u/a_0; \quad \bar{v} = \sqrt{\gamma}\,v/a_0;\\
&\bar{T} = T/T_0; \qquad \bar{\theta} = \theta/T_0;\\
&\tau = a_0 t/\sqrt{\gamma}\,L; \quad \bar{x} = x/L;
\end{aligned}$$

where subscript "0" refers to the flow state originally separating the two oncoming incident shock waves. In the above definitions a is the local speed of sound and γ is the ratio of the

specific heat capacities, i.e., $\gamma = C_p/C_v$. L is a characteristic length. The value of L was chosen to be 1 m. The S_1 shock wave was located 0.266 m from the left end and the S_2 shock wave was located 0.266 from the right end. Thus the distance separating the two incident shock waves was 0.468 m. Only the region between the two incident shock waves was seeded with dust particles. All the calculations were performed with $N = 750$ mesh points. Thus the distance between mesh points of the spatial grid, i.e., $\Delta X = L/N$, was $\Delta X = 1.333 \times 10^{-3}$ m. Although a change in L would imply a different size for the spatial grid, its influence on the final results is negligibly small since a change in ΔX would imply an inverse change in ΔT since the spatial and the time increments are related through the Courant–Friedrichs–Lewy condition (1928), namely:
$\Delta T < \Delta X/\max(|u| + a)$ where a is the local speed of sound and u is the gas velocity. The average running time was 1200 s. CPU on the CDC Cyber 180-840 computer.

3. Results and discussions

3.1. Pure-gas

As a first step, the computer code developed for solving the problem at hand was checked by comparing its results for the case of a head-on collision of normal shock waves in a pure gas with those predicted analytically by Glass (1987), Gould (1952) and Nicholl (1951). Excellent agreement was obtained.

Typical results for the pressure, the temperature and the flow velocity are shown in figs. 2, 3 and 4, respectively. Each of these figures consists of two parts: part (a) prior to, and part (b) after the head-on collision. The Mach number of the incident shock wave propagating from left to right is 3 and that of the one propagating from right to left is 2. The two incident shock

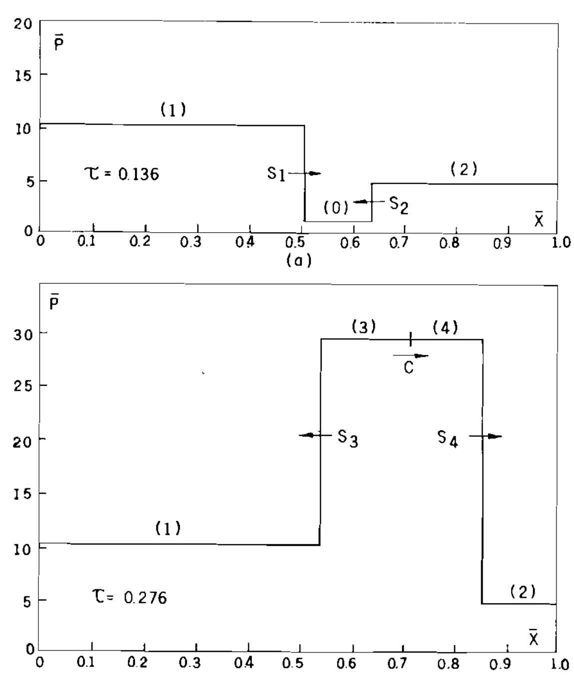

Fig. 2. The pressure history prior to (a) and after (b) the head-on collision for a pure gas.

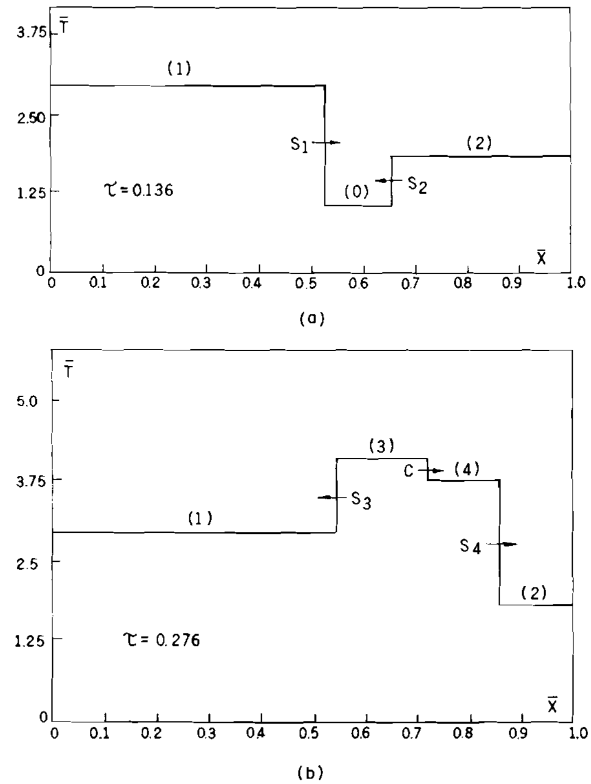

Fig. 3. The temperature history prior to (a) and after (b) the head-on collision for a pure gas.

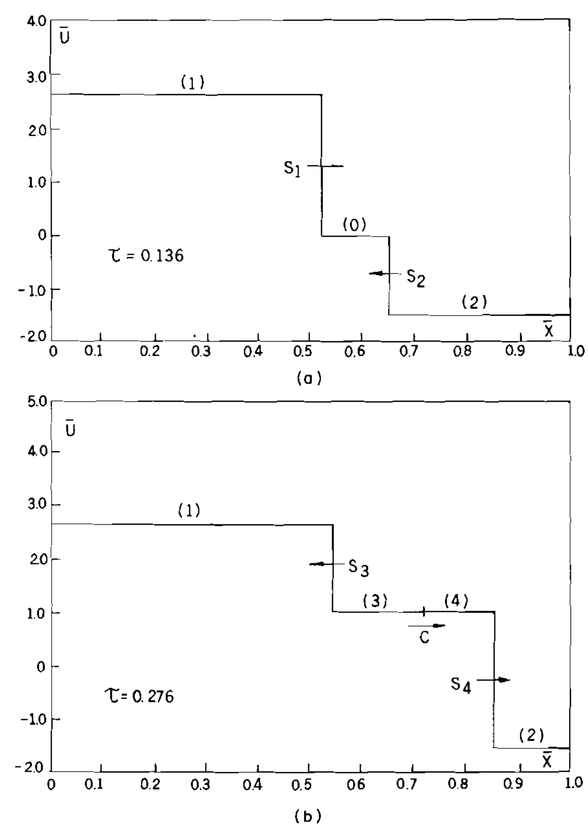

Fig. 4. The velocity history prior to (a) and after (b) the head-on collision for a pure gas.

waves, S_1 and S_2, can be seen in fig. 2a propagating one toward the other. The sharp pressure jumps across them clearly indicate the effectiveness of the random choice method in perfectly describing shock waves. The pressure history after the head-on collision is shown in figure 2b. The pressure jumps across the S_3 and the S_4 shock waves are again seen to be very sharp. Note that since $\bar{P}_3 = \bar{P}_4$, the contact surface separating states (3) and (4) cannot be identified in the pressure profile plot.

Fig. 3(a) illustrates the temperature profile prior to the head-on collision. The sharp jumps across S_1 and S_2 are again clearly seen. In figure 3b, where the temperature profile after the head-on collision is shown, the existence of a contact surface between states (3) and (4) is clearly seen. For this case $\bar{T}_3$ is greater than $\bar{T}_4$.

The shock induced flow velocities behind S_1 and S_2 are shown in fig. 4(a). The flow behind S_1 moves to the right and hence $\bar{u}_1$ is positive while the flow behind S_2 moves to the left and $\bar{u}_2$ therefore, is negative. After the head-on collision (fig. 4(b)) the flow velocities on both sides of the contact surface, which are equal, i.e., $\bar{u}_3 = \bar{u}_4$, are positive, and hence, the contact surface which has the same velocity is following the S_4 shock wave and moving to the right. Note again that due to the boundary condition of equal velocities across the contact surface, it cannot be identified in the velocity profile plot.

It should again be mentioned that since the gas under consideration is a perfect pure gas, the values of the flow properties behind the shock waves and the velocities of the various discontinuities remain constant. Only the distances between the various discontinuities are changing linearly with time.

3.2. The effect of the physical properties of the dust

In the following the effect of the physical properties of the dust, namely; the dust loading ratio, $\beta = \sigma_0/\rho_0$, the diameter of the dust particles, d, and the material density, ρ_s, of the dust particles, on the suspension properties will be investigated. A reference case (labelled by subscript "R") for which the loading ratio $\beta_R = 1$, the diameter of the dust particles is $d_R = 10$ μm and the material density of the dust particles $\rho_{sR} = 2.5$ g/cm^3 will be compared with other combinations. In each of the other combinations only one parameter, either β, d or ρ_s, will be changed. In this way, the dependence of the flow field on the parameter which has been changed can be evaluated. It should be mentioned here, that a detailed solution of the head-on collision of shock waves in a dusty gas with the reference parameters is available in Elperin et al. (1987).

In addition to the above parameters, the following values were used as initial conditions: $P_0 = 1$ atm, $T_0 = 300$ K, $C_m = 800$ J/(kg K), $\gamma = 1.4$. The dynamic viscosity, μ, was calculated using the following expression for air which was given by Miura, Saito and Glass (1986);

$$\mu = 1.71 \times 10^{-5}(T/273)^{0.77},$$

here T should be inserted in K and μ is in kg/(m s). C_p is calculated from;

$$C_p = \gamma\mathscr{R}/(\gamma - 1)M_a,$$

where $\mathscr{R}$ is the universal gas constant [$\mathscr{R} = 8314$ J/(kgmol K)] and M_a is the effective molecular weight of air ($M_a = 29$). The Prandtl number was taken to be equal to 0.75.

Changes in β should in principle cause an effect which could easily be deduced from the work of Elperin et al. (1987), i.e., as β decreases the results should approach asymptotically those appropriate to a pure gas, i.e., $\beta = 0$.

The diameter of the solid particles, d, influences the problem at hand in the following manner. The Reynolds number which depends linearly on d (i.e., $\mathrm{Re} = \rho\,|\,v - u\,|\,d/\mu$) determines the drag coefficient, C_D, and the Nusselt number, Nu. These two parameters determine the drag force, D, which varies as d^2 (see eq. (1a)), and the heat transfer, Q, which varies as d (see eq. (1b)). In addition, the particle volume and hence, mass, varies as d^3 (i.e., $m = \rho_s \pi d^3/6$). Thus the acceleration of the solid particle due to the gas drag force varies as $1/d$, i.e., decreases when the particle diameter is increased. Note also that a change in the diameter of the solid particles, d, while the loading ratio, β, is kept unchanged affects the total number of the solid particles which are contained in the suspension.

Similarly, the material density of the solid particles, ρ_s, also influences their mass, but only linearly, since the mass dependence on the material density is linear. However, unlike changes in the diameter of the solid particles, d, which result in changes in both the mass of the solid particles and the drag force acting on them, the density, ρ_s, affects only the mass of the particles.

The pressure in the flow field prior to the head-on collision, $\tau = 0.176$, is shown in fig. 5a. In each of the three sets of curves the reference curve is drawn with one additional curve in which

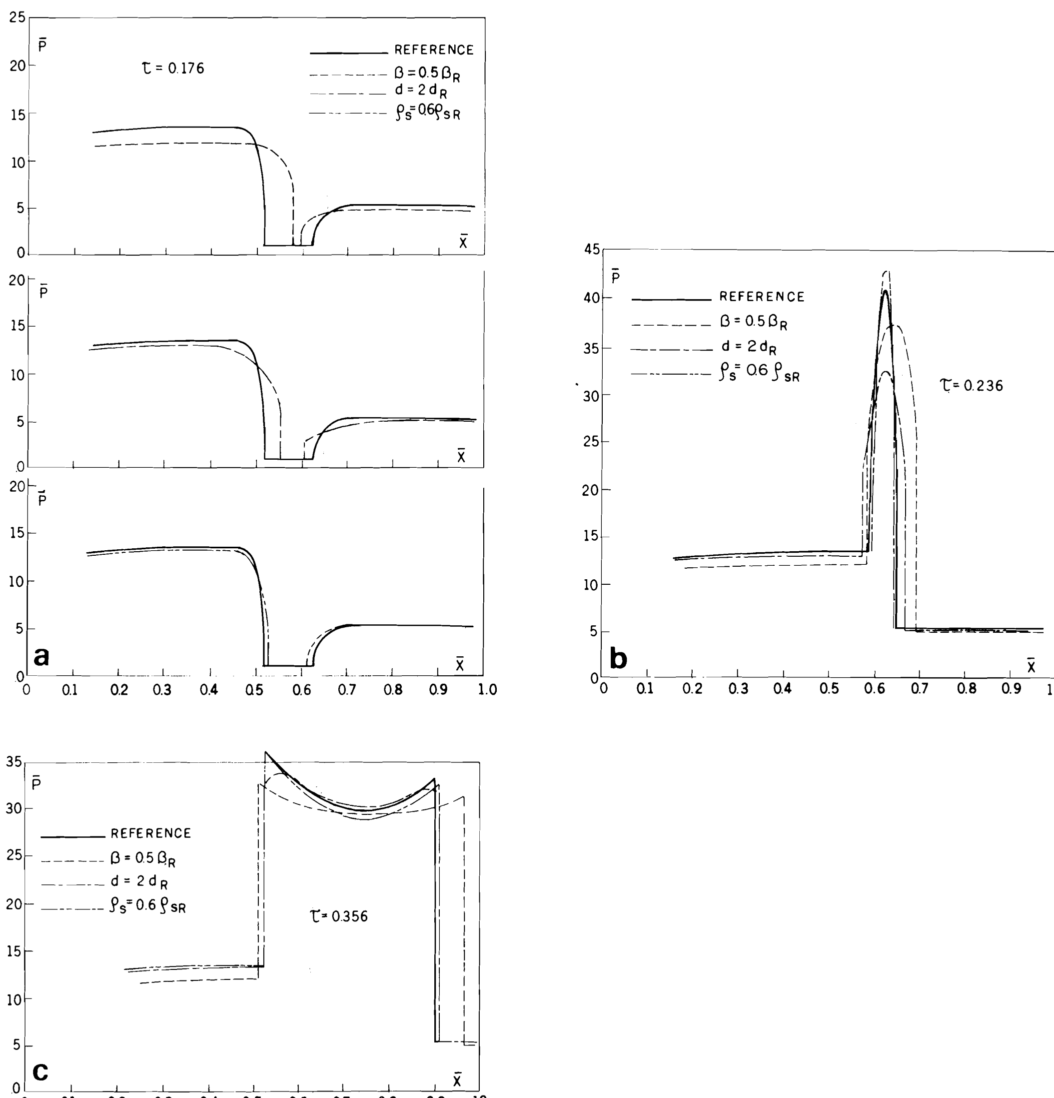

Fig. 5. The dependence of the suspension pressure on the dust properties (a) prior to the head-on collision. (b) immediately after the head-on collision. (c) long after the head-on collision.

one of the parameters has been changed. The case of $\beta = 0.5\beta_R$ is shown at the top of fig. 5a. As expected, the reduction of the loading ratio reduces the maximum pressures obtained behind the incident shock waves which move in this case faster. When the diameter of the solid particles is doubled, i.e., $d = 2d_R$, the incident shock waves move faster and the extent of the relaxation zone (the distance along which the suspension pressure reaches its maximum) increases. This effect can be explained by the decreased acceleration of the solid particles due to the drag force which increases the distances travelled by the solid particles before they reach a state of kinematic equilibrium with the carrying gas.

Reducing the material density of the solid particles by a factor of 0.6, results in minor changes in the pressure profile. The incident shock waves speed up slightly.

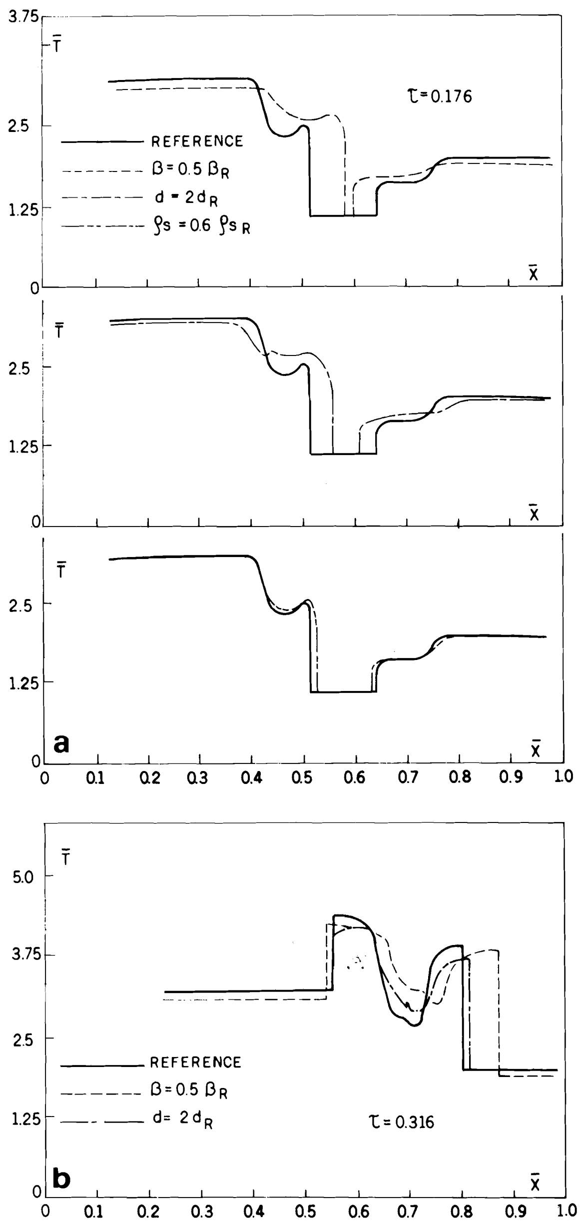

Fig. 6. The dependence of the gas temperature on the dust properties (a) prior to the head-on collision. (b) long after the head-on collision.

The pressure profile immediately after the head-on collision at $\tau = 0.236$ is shown in fig. 5b. A decrease in the loading ratio or an increase in the diameter of the solid particles cause a noticeable decrease in the peak pressure at this time. The material density of the solid particles, however, again is seen to have only a minor affect on the pressure profile.

A long time after the head-on collision, i.e., $\tau = 0.356$ (see fig. 5c), the pressures are seen to attain the same values. In addition, the separation between the reflected shock waves in the case of the reduced dust loading ratio is, as expected, greater, for the reflected shock waves move faster.

The temperature profile prior to the head-on collision, at $\tau = 0.176$, is shown in fig. 6a. At the top of this figure, where the effect of reducing the loading ratio by 50% is illustrated, it can be seen that as β becomes smaller the double-step type profile is smeared out and the shape of the temperature profile approaches the single-step shape typical of a pure gas. The dependence of the gas temperature on the diameter of the solid particles is shown in the center of fig. 6a. When the diameter of the solid particles is doubled the incident shock waves move faster, resulting in higher jumps in the temperature immediately behind them. However, since the initial condition including the loading ratio for the two cases are identical, the temperatures far behind the incident shock waves at the ends of the relaxation zones are independent of the particle diameter.

The effect of the material density of the solid particles on the gas temperature is shown in the bottom of fig. 6a. It is seen again that a reduction in the material density, ρ_s, causes the incident shock waves to speed up. Aside from this effect, the temperature profile is hardly affected. For this reason, i.e., the minor effect of the particle material density on the various flow profiles, in the following discussion the curves for $\rho_s = 0.6\rho_{sR}$ are omitted unless the effect of ρ_s on some properties is more significant than that obtained so far.

Fig. 6b illustrates the temperature profile long time after the head-on collision, $\tau = 0.316$. Again, it is seen that, in general, the temperature profiles at this late time are similar. The reflected shock waves propagating into the suspension with the largest dust loading ratio, i.e., $\beta = \beta_R$, are the slowest. They are faster when the diameter of the solid particles increases and are considerably faster when the loading ratio β is reduced (i.e., $\beta = 0.5\beta_R$).

The gas velocities prior to $\tau = 0.176$, and after, $\tau = 0.316$ head-on collision are shown in figs. 7a and 7b, respectively. It is clear from these figures that a reduction in the loading ratio, β, results in higher velocities. Recall that the velocities in the right hand side of figure 7a are negative, and hence the lowest line corresponds to the highest absolute velocity. It is also evident from these figures that the velocities are higher when the diameter of the solid particles is doubled.

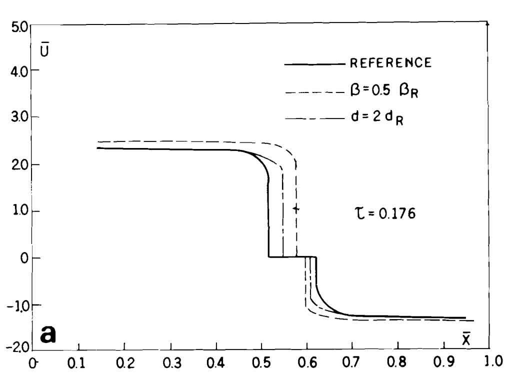

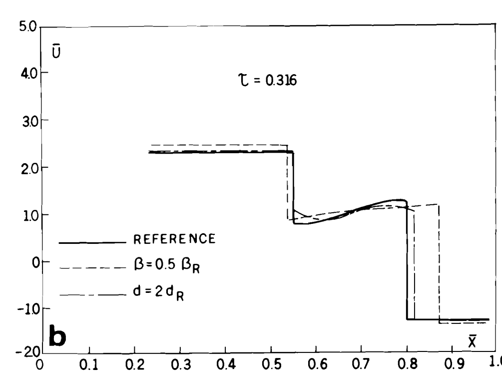

Fig. 7. The dependence of the gas velocity on the dust properties (a) prior to the head-on collision. (b) long after the head-on collision.

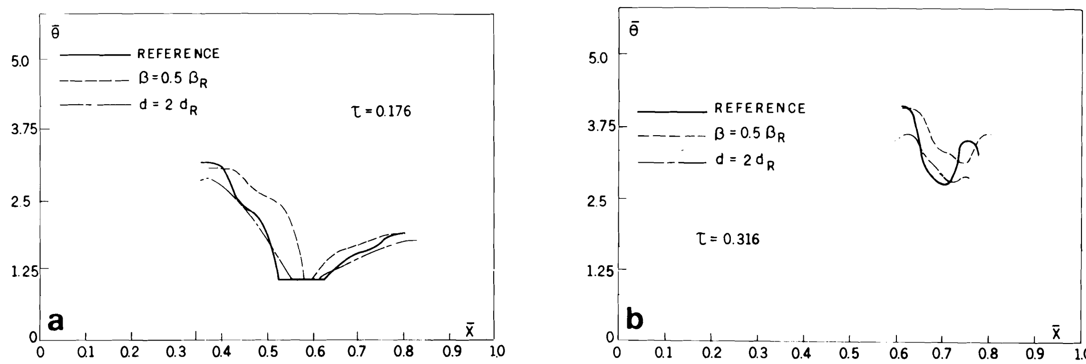

Fig. 8. The dependence of the dust temperature on the dust properties (a) prior to the head-on collision. (b) long after the head-on collision.

The temperature of the solid particles, θ, is shown in figures 8a and 8b which correspond to $\tau = 0.176$, and $\tau = 0.316$, respectively. Since the mass of the solid particle is proportional to d^3 while the surface area available for heat exchange varies as d^2, it is expected that the rise in the temperature of the larger particles will be smaller than that of the smaller particles. This fact can clearly be seen in figures 8a and 8b. Figure 8b also indicates that the largest distance between the edges of the dust cloud corresponds to the suspension having less dust (i.e., $\beta = 0.5\ \beta_R$). This is probably due to the fact that more momentum per mass is transferred to the dust when the loading ratio is reduced and hence, the dust particles attain the kinematic equilibrium with the gas flow generated by the reflected shock waves, faster. On the other hand, when the loading ratio remains the same, but the diameter of the solid particles is doubled, the momentum per mass transferred to the dust particles is the same, but their acceleration varies as $1/d$ which results in a shorter distance between the edges of the dust cloud.

The foregoing discussion concerning the attainability of the kinematic equilibrium between dust particles and gas flow generated by the reflected shock waves is illustrated in figure 9b where the velocity of the dust particles after the head-on collision is shown.

The spatial density of the dust particles $\bar{\sigma}$, for $\tau = 0.176$, and $\tau = 0.316$ is shown in figs. 10a and b, respectively. Since the two incident shock waves induce two flows in states (1) and (2) which move one toward the other the dust particles are initially swept toward the location where the head-on collision takes place, and hence the spatial density of the dust starts to increase behind the shock fronts as shown in fig. 10a. Long after the head-on collision, the

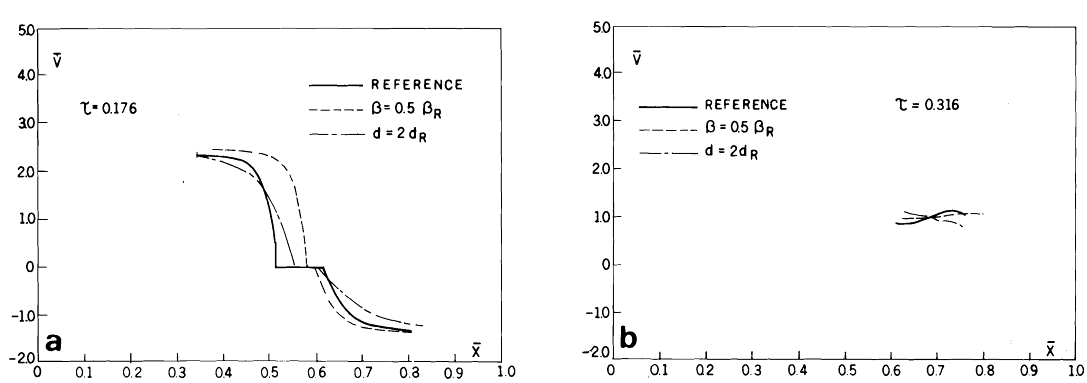

Fig. 9. The dependence of the dust velocity on the dust properties (a) prior to the head-on collision. (b) long after the head-on collision.

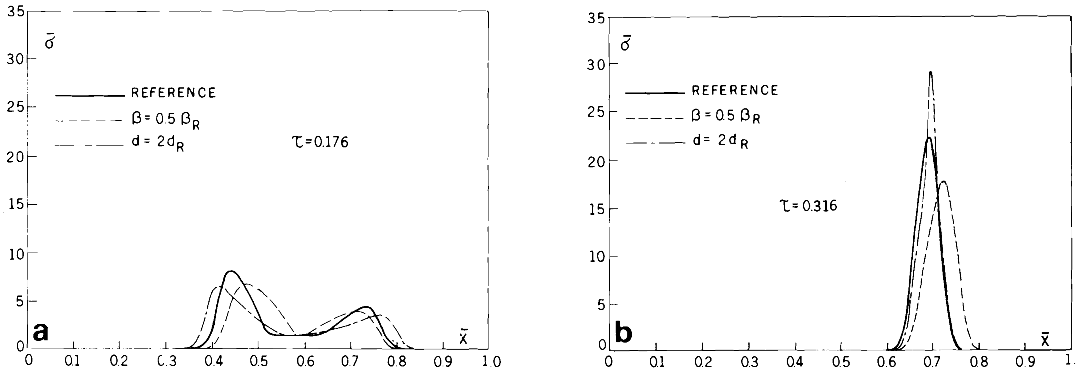

Fig. 10. The dependence of the dust spatial density on the dust properties (a) prior to the head-on collision. (b) long after the head-on collision.

entire flow between the two reflected shock waves moves to the right (see fig. 9b) resulting in a spike-like shape in the profile of the spatial density. In view of the earlier discussion, the effect of the dust physical properties on the spatial density shown in these figures are self-explanatory. However, it should be mentioned that after the head-on collision, fig. 10b, the highest spatial density is obtained for the case $d = 2d_R$, which corresponds to a smaller number density of the solid particles, while the lowest spatial density is obtained for the case $\beta = 0.5\ \beta_R$, which corresponds to a smaller mass of the solid phase in the suspension, as compared to the reference case.

4. Conclusions

The effect of the various physical dust parameters, namely: the diameter of the solid particles, the material density of the solid particles, and the loading ratio of the solid phase in the suspension on the flow field generated by the head-on collision of two normal shock waves in a dusty gas were investigated numerically using the modified random choice method (RCM).

It has been shown that while the flow field properties are sensitive to the loading ratio and the diameter of the solid particles, they are relatively insensitive to the material density of the solid particles.

As expected, reduction in the loading ratio results in an approach to the case appropriate to a pure gas.

Reduction in the diameter of the solid particles causes a reduction of the relaxation time required for the solid particles to attain the kinematic equilibrium with the carrying gas. Consequently, the relaxation lengths are much shorter and the attenuation of the shock waves is smaller. This in turn results in higher pressures and densities in the flow field.

The present numerical study complements a previous one in which the head-on collision of two normal shock waves in a dusty gas was investigated, since the previous study did not include an investigation of the effect of the physical parameters of the solid particles on the suspension flow field.

References

Anderson, J.B. (1982) *Modern Compressible Flow*, 1st ed. (McGraw-Hill, New York).
Carrier, G.F. (1958) Shock Waves in Dusty Gases, *J. Fluid Mech. 4*, 376–382.

Courant, R., Friedrichs, K.O. and Lewy, H. (1928) On the Partial Difference Equations of Mathematical Physics, *Math. Ann. 100*, 32–74.

Elperin, T. and Igra, O. (1986) About the Choice of Uniformly Distributed Sequences to be Used in the Random Choice Method, *Comp. Methods Appl. Mech. Eng. 57*, 181–189.

Elperin, T., Ben-Dor, G. and Igra, O. (1987) Head-On Collision of Normal Shock Waves in Dusty Gases, *Int. J. Heat & Fluid Flow 8*, 303–312.

Glass, I.I. (1987) Private communication.

Godunov, S.K. (1959) Finite Difference Method for Numerical Calculations of Discontinuous Solutions of Equations of Hydrodynamics, *Math. Sbornik 47*, 271–306 (in Russian).

Gould, D.G. (1952) The Head-On Collision of Two Shock Waves and a Shock and Rarefaction Wave in One-Dimensional Flow, *UTIAS Review No. 17*.

Igra, O. and Ben-Dor, G. (1980) Parameters Affecting the Relaxation Zone Behind Normal Shock Waves in Dusty Gas, *Israel J. Tech. 18*, 159–168.

Kraiko, A.N. (1979) On Discontinuity Surfaces in a Medium Devoid of Proper Pressure, *Appl. Math. Mech. 43*, 539–549.

Kraiko, A.N. (1982) The Two-Fluid Model of Flow of Gas with Particles Dispersed in It, *Appl. Math. Mech. 46*, 96–106.

Kriebel, A.R. (1964) Analysis of Normal Shock Waves in a Particle Laden Gas, *J. Basic Eng., Trans. ASME, Ser. D86*, 655–663.

Marble, F.E. (1970) Dynamics of Dusty Gases, *Ann. Rev. Fluid Mech. 2*, 397–446.

Miura, H. and Glass, I.I. (1983) On the Passage of a Shock Wave through a Dusty Layer, *Proc. Roy. Soc. Lond., Ser. A385*, 85–105.

Miura, H., Saito, T. and Glass, I.I. (1986) Shock Wave Reflection from a Rigid Wall in a Dusty Gas, *Proc. Roy. Soc. Lond. A404*, 55–67.

Morgenthaler, J.H. (1962) Analysis of Two-Phase Flow in Supersonic Exhausts, *Progress in Astronautics and Rocketry*, vol. 6, eds. S.S. Penner and F.A. Williams (Academic Press, New York) 145–163.

Nicholl, C.I.H. (1951) The Head-On Collision of Shock and Rarefaction Waves, *UTIAS Report No. 10*.

Rudinger, G. (1964) Some Properties of Shock Relaxation in Gas Flows Carrying Small Particles, *Phys. Fluids 7*, 658–663.

Rudinger, G. (1973) Wave Propagation in Suspensions of Solid Particles in Gas Flow, *Appl. Mech. Rev. 26*, 273–279.

Saito, T. and Glass, I.I. (1984) Applications of Random Choice Method to Problems in Gasdynamics, *Prog. Aero. Sci. 21*, 201–247.

Schmitt-von Schubert, B. (1969) Existence and Uniqueness of Normal Shock Waves in Gas-Particle Mixtures, *J. Fluid Mech., 38*, 633–655.

Sommerfeld, M. (1985) The Unsteadiness of Shock Waves Propagating through Gas-Particle Mixtures, *Experiments in Fluids 3*, 197–206.

Soo, S.L. (1967) *Fluid Mechanics of Multiphase Systems*, (Blaisdell, Waltham, Mass).